

Systematic improvement of molecular representations for machine learning models

Bing Huang and O. Anatole von Lilienfeld*

*Institute of Physical Chemistry and National Center for Computational Design and Discovery of Novel Materials (MARVEL),
Department of Chemistry, University of Basel, Klingelbergstrasse 80, 4056 Basel, Switzerland*

(Dated: May 19, 2022)

The predictive accuracy of Machine Learning (ML) models of molecular properties depends on the choice of the molecular representation. We introduce a hierarchy of representations based on uniqueness and target similarity criteria. To systematically control target similarity, we rely on interatomic many body expansions including Bonding, Angular, and higher order terms (BA). Addition of higher order contributions systematically increases similarity to the potential energy function as well as predictive accuracy of the resulting ML models. Numerical evidence is presented for the performance of BAML models trained on molecular properties pre-calculated at electron-correlated and density functional theory level of theory for thousands of small organic molecules. Properties studied include enthalpies and free energies of atomization, heatcapacity, zero-point vibrational energies, dipole-moment, polarizability, HOMO/LUMO energies and gap, ionization potential, electron affinity, and electronic excitations. After training, BAML enables predictions of energies or electronic properties of out-of-sample molecules with unprecedented accuracy and speed.

Reasonable predictions of ground-state properties of molecules require computationally demanding calculations of approximated expectation values of the corresponding operators. [1] Alternatively, Kernel-Ridge-Regression based ML models [2] can also *infer* the observable in terms of a linear expansion in chemical compound space, $O^{\text{inf}}(\mathbf{M}) = \sum_i^N \alpha_i k(d(\mathbf{M}, \mathbf{M}_i))$, where k is the kernel function (often Gaussian or exponentially decaying), d is a metric, and \mathbf{M} is the molecular representation i used for training to obtain regression weights $\{\alpha_i\}$. Once trained, the advantage of such ML methods consists of their computational efficiency with multiple orders of speed-up with respect to conventional quantum chemistry methods. Their drawback is that they (a) are incapable of extrapolation by construction, and (b) require substantial training data before reaching satisfying predictive power for out-of-sample molecules. In practice, addressing (a) is less important since one typically knows beforehand which ranges of interatomic distances and chemical compositions are relevant to the chemical problem at hand: It is straightforward to impose the appropriate domain of applicability for the application of supervised ML models in chemistry. In recent years, much work has been devoted to tackle the latter drawback through the discovery and development of improved representations \mathbf{M} for use in ML models of quantum chemical properties of molecules and materials [5–11].

Often, new descriptors are introduced based on *ad hoc*/trial-and-error reasoning, such as using features which characterize a system or the property of interest, which meet known invariances, which simply add “more of the physics”, or which simply encode anything which could possibly be related to the system of interest. The use of new representations is justified *a posteriori*: They yield ML models with good performance.

Severe survivorship bias, however, is likely to occur: Alternative representations which could have been obtained from the same set of guidelines, and which result in poor ML model performance, are not reported. While such practice is not wrong it is questionable if it is ideal: Arbitrarily many different representations could have been designed using the exact same guidelines. Unfortunately, and to the best of our knowledge, there is no general specific and rigorous procedure for systematically optimizing molecular representations for converged and robust ML model performance *without* heavy numerical experimentation and conclusions drawn *a posteriori*. In this paper, we use arguments based on quantum mechanics to identify a hierarchy of representations which enable the generation of ML models with systematically increased predictive accuracy. To support our findings, we present numerical evidence for multiple ML models using the same set of quantum chemical ground-state properties and structures, previously calculated for thousands of organic molecules [14]

For large N , errors of decent ML models must decay as inverse roots of N [2], leading to a linear relationship, $\log(\text{Error}) = a - b \log(N)$. Therefore, the best representation must (i) minimize the off-set a and (ii) preserve the linearity in the second term while maximizing its pre-factor b . According to the first postulate of quantum mechanics any system is represented by its wavefunction Ψ which results from applying the variational principle to the expectation value of the Hamiltonian operator. As such, there is a one-to-one relationship between Hamiltonian and Ψ . While some representations have been introduced in order to mimic Ψ (or its electron density) [15], we rather focus on directly modeling the Hamiltonian/Energy of the system. More specifically, we investigate the effect of using increasingly higher orders in a many-body potential energy expansion in order to (i) maximize similarity between representation and target function and to (ii) introduce one-to-one uniqueness [5].

We exemplify the importance of target similarity for a

* anatole.vonlilienfeld@unibas.ch

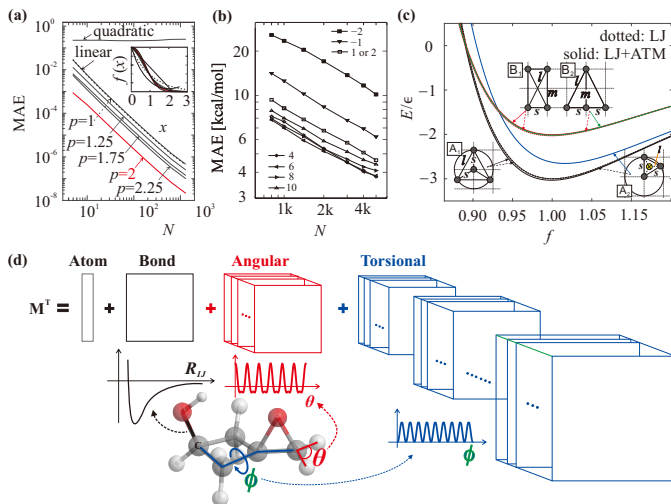


Figure 1. Target similarity determines offset a in ML model learning curves $\log(\text{Error}) = a - b \log(N)$. Panels (a) and (b) illustrate curves for ML models obtained for various representations applied to learning a 1-D Gaussian target function or enthalpy of atomization for QM7b dataset [4]. (a) shows learning curves using linear, quadratic, and various exponential representations. The inset shows the target function as well as the representations. (b) shows learning curves using several adapted Coulomb matrices with off-diagonal elements defined as $Z_I Z_J / R_{IJ}^n$, where n is specified in the legend. (c) Illustration that 3-body interactions are not negligible for describing two pairs of homometric Ar_4 clusters: group A (A_1 and A_2 , where $l = \sqrt{3}s$) and group B (B_1 and B_2 , where $m = 2s, l = \sqrt{5}s$). The horizontal axis label f corresponds to isotropic scaling of s with $f = 1$ corresponding to $s = 3.82 \text{ \AA}$. LJ and ATM represent resulting Lennard-Jones potential and Axilrod-Teller-Muto 3-body potential [12, 13], respectively. (d) Illustration of the UFF based constructin of BAML.

mock supervised learning task: Modeling a 1D Gaussian function (Inset Fig. 1(a)). As representations \mathbf{M} we use linear, quadratic, and exponentially decaying functions with varying exponent of x . The learning curves of the ML models (Fig. 1(a)) indicate systematic improvement as the target similarity of the representation increases. Note that all learning curves, with the notable exception of the quadratic one, exhibit the same slope b on the log-log plot of the learning curve: They only differ in learning curve off-set a . When using a Gaussian function as a representation, the smallest off-set is observed. It is easy to see why the error of the ML model using the quadratic function as a representation does not decrease when adding more training data: Its minimum is at $x = 0$, and in the region $x > 2$ the function turns upward again, preventing a one-to-one map between x and representation. In other words, the quadratic function is not monotonic and therefore lacks uniqueness, introducing noise in the data which leads to an error converging to a finite residual value, rather than to zero. All other functions are monotonic and conserve the one-to-one map to x . As such, they are unique representations and they

reduce the logarithm of the error in a linear fashion at the same rate as the amount of training data grows. While the rate appears to be solely determined by the uniqueness of the representation, implying that uniqueness is a necessary condition for a functional descriptor, the off-set of the resulting model appears to be solely determined by target similarity.

To see if this argument also holds for real molecules, we have applied a set of unique representations with differing target similarity to model atomization energies in organic molecules. More specifically, learning curves have been obtained using atom adjacency matrices based on the recently introduced Coulomb matrix [3], with off-diagonal elements $M_{IJ} = Z_I Z_J / R_{IJ}^n$. Where R_{IJ} is the interatomic distance between atoms I and J , and the conventional Coulomb matrix is recovered for $n = 1$. For any non-zero choice of n these matrices encode the complete polyhedron defined in the high-dimensional space spanned by all atoms in the molecules: They uniquely encode the molecule’s geometry and composition. For negative n values, however, this representation becomes unphysical because the magnitude of its off-diagonal elements *increases* with interatomic distance. Corresponding learning curves shown in Fig. 1(b) reflect this fact: As off-diagonal elements become increasingly unphysical by dialing in square-root, linear, and quadratic functions in interatomic distance, respectively, the off-set a increases as well. Conversely, matrix representations with off-diagonal elements which follow the Coulomb and higher inverse power laws are more physical and exhibit lower off-sets. We note again that independent of the representation’s target similarity, the learning rate (slope of log-log error-training set size curve) corresponds to the same constant, reflecting the fact that all these representations are unique.

The bag-of-bond (BoB) representation, a stripped down pair-wise variant of the Coulomb matrix, has resulted in remarkably predictive ML models [16]. We use it as a starting point for the development of our systematically improved representation. Unfortunately, when relying on a pair-wise two-body bag of bond representation the uniqueness requirement can be violated by arbitrarily many sets of geometries, no matter how strong the target similarity of the employed functional form. In Fig. 1(d), we demonstrate this flaw for two pairs of homometric molecules, each with four rare gas atoms, once in a competition of a pyramidal/planar geometry (A), and once for a rectangular/triangular pair (B). Both pairs exhibit the exact same list of interatomic distances: $3s/3l$ for A, and $2s/2m/2l$ for B. Consequently, when using a pair-wise energy expression (no matter how effective), the predicted curve as a function of a global scaling factor f will be indistinguishable for both pairs (shown in Fig. 1(d) using Lennard-Jones potentials with parameters for Argon). Only after the addition of the corresponding three-body van der Waals Axilrod-Teller-Muto [12, 13] contribution, the homometric pairs can be distinguished. As a side-note, this simple example also underscores the qual-

itative importance of many-body contributions in interatomic energy decompositions which plays a role even in effects as weak as London dispersion forces—in addition to the already established quantitative role they play in nature [17, 18]

Using the insight gained, we have investigated a hierarchy of representations which consists of bags of (1) dressed atoms (\mathbf{M}^D), (2) atoms and bonds (\mathbf{M}^B), (2) bags of atoms, bonds and angles (\mathbf{M}^A), and (3) bags of atoms, bonds, angles, and torsions (\mathbf{M}^T). To indicate the many-body expansion character we dub these feature vectors the “BA-representation” (standing for bags of Bonds, Angles, Torsions, etc. pp.). For this work, we have used functional forms and parameters for BA-representations that correspond to the universal force field (UFF) [19]. The corresponding terms are illustrated in Fig. 1(d), and correspond to averaged atomic contributions to energies of molecules in training set for atoms, Morse potentials for bonds, and sinusoidal functions for angles and torsions. While we find that use of the UFF results in consistent and remarkable performance, we note that other force fields could have been used just as well. In particular, we also tested the use of Lennard-Jones and Axilrod-Teller-Muto functions in BA based ML models (BAML), and found systematic improvement and remarkable performance also for these functional forms and dispersion coefficients.

We tested UFF based BAML using three previously established data sets: DFT energies and properties of $\sim 7k$ organic molecules stored in the QM7b data set (introduced in Ref. [4]), G4MP2 energies and DFT properties for 6k constitutional isomers of $C_7H_{10}O_2$, and DFT energies and properties for 134k organic molecules QM9 (both published in Ref. [14]). Links to all data sets are available at <http://quantum-machine.org>. Initial structures for all datasets were drawn from the GDB universe [20, 21].

Log-log plots of BAML learning curves are shown in Fig. 2(a) and (b) for the $C_7H_{10}O_2$ isomers as well as for QM9. Mean absolute errors (MAEs) for out of sample predictions of nine properties are shown as a function of training set size for the BAML model. Properties studied include enthalpies and free energies of atomization at room temperature, heat-capacity at room temperature C_V , zero-point-vibrational-energy (ZPVE), norms of dipole moments μ and polarizability α , as well as HOMO/LUMO eigenvalues and gap. For every property, we find near identical learning rates for BAML models based on bonds (\mathbf{M}^B), bonds+angles (\mathbf{M}^A), or atoms+bonds, angles+torsions (\mathbf{M}^T). The learning offset a , however, decreases systematically as target similarity is being increased through the addition of higher order contributions—for all properties, and for both data sets. This observation confirms the expectations raised based on the aforementioned arguments. We note that BAML can reach chemical accuracy (MAE ~ 1 kcal/mol with respect to reference) for atomization energies of the isomers of $C_7H_{10}O_2$ after training on only 5k example molecules, and MAE ~ 2.4 kcal/mol for 124k organic molecules in

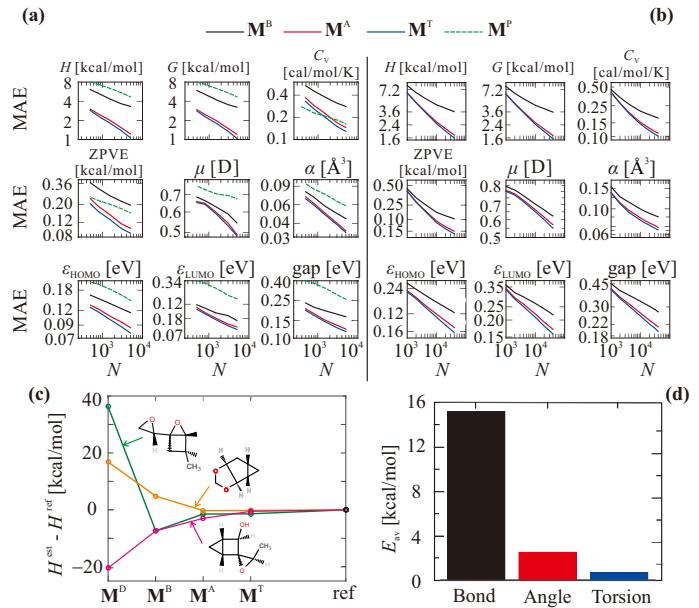


Figure 2. (a): BAML and polarizability representation based ML learning curves for 9 molecular properties of 6k constitutional isomers of formula $C_7H_{10}O_2$ [14]. (b) BAML learning curves for 134k QM9 molecules for the same 9 molecular properties [14]. Property models trained include H , G , C_V , ZPVE, μ , α , ϵ_{HOMO} and ϵ_{LUMO} , i.e. enthalpy (kcal/mol), free energy (kcal/mol), heat capacity (cal/mol/K), zero point vibrational energy (kcal/mol), dipole moment (Debye), polarizability (\AA^3), HOMO energy (eV) and LUMO energy (eV), respectively. All errors in (a) and (b) must be divided by 10. Panel (c) shows convergence of estimated enthalpy values to reference values (all shifted towards zero) for three most extreme outlier isomers in $C_7H_{10}O_2$ set. Panel (d) is the averaged “contribution” of each order type in a many-body potential, i.e., the bond, angle and torsion part.

QM9 after training on 10k example molecules. To the best of our knowledge, such predictive power has not yet been reached by any other ML model.

In Fig. 2(c) we quantify the individual contributions for bonds, angles, and torsion by examining the atomization energy of three $C_7H_{10}O_2$ outliers for which the out-of-sample error is maximal. In all three cases, the molecules experience high internal strain through few membered or joint hetero cycles. As such, one would expect substantial lowering of the error when taking into account angular, and torsional contributions. And indeed, for all three molecules, the addition of the higher order terms leads to systematically reduced errors. Fig. 2(d) indicates the averaged contribution to the atomization energy coming from BAML models using bonds, bonds+angles, or bonds+angles+torsion (always including dressed atom terms). Not surprisingly, these contributions decrease systematically. Their magnitude, however, is still very substantial for angles (~ 3 kcal/mol), and not negligible for torsion (~ 0.5 kcal/mol). Note that the last term might appear small, however, this is only on average—meaning that it can be substantially larger under certain

circumstances, such as the outliers shown in Fig. 2(c).

In order to critically examine our uniqueness and target similarity hypothesis, we have performed an additional test: We constructed a molecular representation which reaches high target similarity with another property, polarizability, but which fails the uniqueness criterion. Instead of using bags of interatomic energy contributions we have used a bag of atomic polarizabilities. Atomic polarizabilities can easily be obtained from Cartesian coordinates of a molecule, i.e. without electronic structure calculations, through the use of Voronoi polyhedra. [18] The resulting representation (\mathbf{M}^P) is a decent model of polarizability, yet it is not unique: Any other molecule which happens to have the same set of atomic polarizabilities will yield the same representation, no matter the differences in geometry. Learning curves obtained for \mathbf{M}^P based ML models are shown together with BAML in Fig. 2(a) for all constitutional isomers. All BAML models have lower learning curves for all properties except for the bond based BAML models of the ZPVE and C_V . In the case of the latter, and for very small unconverged training set sizes, the polarizability ML model is even better than any BAML model. This observation also underscores the necessity to take the convergence behavior of ML models into consideration: Learning rates can differ in a and b . We note the tendency of the polarizability based ML model to exhibit a smaller rate (C_V , ZPVE, μ , α), indicating the expected lack of uniqueness. In particular, even for the target property polarizability the polarizability based representation results in worse ML models than all BAML models. This finding confirms the idea that Hamiltonian/ Ψ /Potential Energy Surface are “special” in that all other molecular properties can be derived from them.

Finally, to place the BAML performance into perspective, we have also compared its out-of-sample errors to literature results obtained using alternative ML models and representations applied to the same molecular data sets. Tab. I displays MAEs and RMSE of the \mathbf{M}^T based BAML model trained on 5k molecules drawn from the QM7b data set. In particular, we compare to KRR ML results obtained using the BoB [16](this work), SOAP [15], and sorted Coulomb matrix (this work). SOAP represents a recently introduced sophisticated convolution of kernel, metric and representation. Results for randomized Coulomb matrices used in a neural network based ML model [4] are also included. BAML yields a MAE for atomization energy of

only ~ 1 kcal/mol, only slightly worse than SOAP’s ~ 0.8 kcal/mol. We note, however, that BAML has a relatively larger RMSE for this property. Similar observations hold for the polarizability, BAML is slightly worse than SOAP. For HOMO/LUMO eigenvalues, ionization potential, and electron affinity, BAML yields lowest MAE and lowest RMSE. BAML also has the lowest MAE for predicting the first excitation energy (together with the randomized neural network based Coulomb matrix model). The lowest RMSE, however, is obtained for BoB. The excitation energy of the most intense peak in the model is predicted with the lowest MAE and RMSE when using the randomized neural network based Coulomb matrix model. BAML is second for MAE, and third for RMSE (after BoB). Finally, the intensity of the most intense peak is best predicted by BAML in terms MAE and RMSE.

In conclusion, we have presented arguments and numerical evidence in support of the notion that a and $b \log N$ in learning curves are influenced, if not determined, by the employed representation’s target similarity and uniqueness, respectively. For molecules, defined by their Hamiltonian which produces their wavefunction which produces the observables, BAML models—based on universal force-field parameters and functions for bags of bonds, angles, and torsions—exhibit uniqueness as well as considerable target similarity. Addition of higher-order contributions in the form of bonds, angles, and torsional degrees of freedom enables the systematic lowering of learning curve off-set a , resulting in BAML models with unprecedented accuracy, transferability, and speed.

Technical details

(229 molecules out of 133885 molecules dissociated after optimization, so are not considered)

ACKNOWLEDGMENTS

O.A.v.L. acknowledges funding from the Swiss National Science foundation (No. PP00P2_138932, 310030_160067). This research was partly supported by the NCCR MARVEL, funded by the Swiss National Science Foundation. Calculations were performed at sciCORE (<http://scicore.unibas.ch/>) scientific computing core facility at University of Basel.

[1] A. Szabo and N. S. Ostlund, *Modern quantum chemistry: introduction to advanced electronic structure theory* (Courier Corporation, 1989).
 [2] K.-R. Müller, M. Finke, N. Murata, K. Schulten, and S. Amari, *Neural Computation* **8**, 1085 (1996).
 [3] M. Rupp, A. Tkatchenko, K.-R. Müller, and O. A. von Lilienfeld, *Physical Review Letters* **108**, 058301 (2012).

[4] G. Montavon, M. Rupp, V. Gobre, A. Vazquez-Mayagoitia, K. Hansen, A. Tkatchenko, K.-R. Müller, and O. A. von Lilienfeld, *New Journal of Physics* **15**, 095003 (2013).
 [5] O. A. von Lilienfeld, R. Ramakrishnan, M. Rupp, and A. Knoll, *International Journal of Quantum Chemistry* **115**, 1084 (2015).

Table I. Mean absolute errors (MAEs) and root mean square errors (RMSE) for the KRR estimation of 14 molecular properties, together with previously published estimation [4],[15] for the same dataset. Errors in the KRR estimation refer to a test set of 2200 randomly selected configurations, while the remaining structures were used for training. Property labels refer to the level of theory and molecular properties, i.e. atomization energy (E), averaged molecular polarizability (α), HOMO and LUMO eigenvalues, ionization potential (IP), electron affinity (EA), first excitation energy (E_{1st}^*), excitation frequency of maximal absorption (E_{max}^*) and the corresponding maximal absorption intensity (I_{max}).

property	mean	BAML		BoB		SOAP [15]		rand CM [4]		CM		accuracy [4]
		MAE	RMSE	MAE	RMSE	MAE	RMSE	MAE	RMSE	MAE	RMSE	
E (PBE0) [kcal/mol]	-36049.85	1.15	2.54	1.84	4.15	0.92	1.61	3.69	8.30	3.69	5.77	3.46, 5.30, 2.08-5.07
α (PBE0) [\AA^3]	11.11	0.07	0.12	0.09	0.13	0.05	0.07	0.11	0.18	0.13	0.19	0.05-0.27, 0.04-0.14
HOMO (GW) [eV]	-209.62	0.10	0.16	0.15	0.20	0.12	0.17	0.16	0.22	0.22	0.29	-
LUMO (GW) [eV]	17.99	0.11	0.16	0.16	0.22	0.12	0.17	0.13	0.21	0.21	0.27	-
IP (ZINDO) [eV]	213.77	0.15	0.24	0.20	0.28	0.19	0.28	0.17	0.26	0.33	0.44	0.20, 0.15
EA (ZINDO) [eV]	12.68	0.07	0.12	0.17	0.23	0.13	0.18	0.11	0.18	0.31	0.40	0.16, 0.11
E_{1st}^* (ZINDO) [eV]	128.68	0.13	0.51	0.21	0.30	0.18	0.41	0.13	0.31	0.42	0.57	0.18, 0.21
E_{max}^* (ZINDO) [eV]	203.39	1.35	1.98	1.40	1.91	1.56	2.16	1.06	1.76	1.58	2.05	-
I_{max} (ZINDO)	0.33	0.07	0.11	0.08	0.12	0.08	0.12	0.07	0.12	0.09	0.13	-

- [6] L. M. Ghiringhelli, J. Vybiral, S. V. Levchenko, C. Draxl, and M. Scheffler, Phys. Rev. Lett. **114**, 105503 (2015).
- [7] J. Behler, The Journal of Chemical Physics **134**, 074106 (2011).
- [8] F. Faber, A. Lindmaa, O. A. von Lilienfeld, and R. Armiento, International Journal of Quantum Chemistry **115**, 1094 (2015).
- [9] A. P. Bartók, R. Kondor, and G. Csányi, Phys. Rev. B **87**, 184115 (2013).
- [10] K. T. Schütt, H. Glawe, F. Brockherde, A. Sanna, K. R. Müller, and E. K. U. Gross, Phys. Rev. B **89**, 205118 (2014).
- [11] V. Botu and R. Ramprasad, International Journal of Quantum Chemistry **115**, 1074 (2015).
- [12] B. M. Axilrod and E. Teller, The Journal of Chemical Physics **11**, 299 (1943).
- [13] Y. Muto, J. Phys.-Math. Soc. Japan. **17**, 629 (1943).
- [14] R. Ramakrishnan, P. O. Dral, M. Rupp, and O. A. von Lilienfeld, Scientific Data **1**, EP (2014).
- [15] S. De, A. P. Bartók, G. Csányi, and M. Ceriotti, Phys. Chem. Chem. Phys. **18**, 13754 (2016).
- [16] K. Hansen, F. Biegler, R. Ramakrishnan, W. Pronobis, O. A. von Lilienfeld, K.-R. Müller, and A. Tkatchenko, The Journal of Physical Chemistry Letters **6**, 2326 (2015).
- [17] R. A. DiStasio, O. A. von Lilienfeld, and A. Tkatchenko, Proceedings of the National Academy of Sciences **109**, 14791 (2012).
- [18] T. Bereau and O. A. von Lilienfeld, The Journal of Chemical Physics **141**, 034101 (2014).
- [19] A. K. Rappe, C. J. Casewit, K. S. Colwell, W. A. G. III, and W. M. Skiff, Journal of the American Chemical Society **114**, 10024 (1992).
- [20] L. Ruddigkeit, R. van Deursen, L. C. Blum, and J.-L. Reymond, Journal of Chemical Information and Modeling **52**, 2864 (2012).
- [21] T. Fink, H. Bruggesser, and J.-L. Reymond, Angewandte Chemie International Edition **44**, 1504 (2005).